ALEPH 95-064
PHYSIC 95-059
P.Odier
7 June 1995

# Measurement of the $\pi^0$ inclusive spectrum in hadronic decays of the $Z^0$

Philippe ODIER

LAPP Annecy

## Abstract

The $\pi^0$ inclusive spectrum is measured with $\pi^0$'s reconstructed from one converted photon (conv.) and one photon measured in the ECAL (GAT), as well as 2 photons measured in the ECAL. The $\pi^0$ signal is extracted by fitting GAT/conv and GAT/GAT invariant mass distributions. The inclusive $\pi^0$ energy spectrum is measured beyond 1 GeV and compared to the predictions from the HVFL generator. The $\pi^0$ transverse momentum and rapidity spectra are also measured.

# 1. Introduction

The $\pi^0$'s produced in hadronic events are expected to have similar spectrum as charged pions, therefore an average energy around 2.2 GeV. Their decay into two photons will give photons in an energy range below 2 GeV. In that region, determining the reconstruction efficiency of photons in the ECAL deserves a dedicated study which is presented in this note. As the photon deposition in that region is not perfectly reproduced by the detector simulation, data themselves have been used to determine the efficiency measurement.

In a first step, $\pi^0$'s are reconstructed from a converted photon (called "conv") and an calorimetric photon (called "GAT") in order to get photon efficiency measurement, which is used in section 6 to reconstruct $\pi^0$'s from two calorimetric photons. Both approaches give results on the $\pi^0$ flux, the larger energy range being covered by the conv/GAT method, which happens to be more precise in terms of systematics.

# 2. Event selection

Hadronic events are taken from the standard hadronic selection (CLAS 16), which corresponds to the following cuts:

at least 5 charged tracks in the TPC with :
- $| D_0 | < 2$ cm
- $| Z_0 | < 10$ cm
- number of TPC coord. $\geq 4$
- $| \cos \theta | < 0.95$

and the total energy of these selected tracks must be more than 10% of $E_{cm}$

An additional cut has been set :

$$35° < \theta_{thrust} < 145°$$

to eliminate events too close to the beam axis.

Below are the statistics used for each data set:

| | 92 | 93 | 94 |
|---|---|---|---|
| data | 527 k | 532 k | 892 k |
| MC | 533 k | 697 k | same events as 93 |

# 3. Selection of converted photons

## 3.1. Electron selection

All charged tracks with Pt w.r.t. beam axis > 140 MeV (in order to eliminate poorly measured tracks) are accepted and the three standard estimators are used to identify electrons: RI (dE/dx in the TPC), RT and RL (transversal and longitudinal shape of the shower in the ECAL).

The distributions of the 3 estimators are shown in fig. 1. The following selection cuts have been defined (based on an optimisation of the signal/noise rate and efficiency):

$$-2.5 < RI < 3$$

$$-2.5 < RT$$

$$-2.5 < RL < 3$$

For P (electron) < 1 GeV, only the first cut is required, as the electron may not reach the ECAL.

For P (electron) > 1 GeV, the charged tracks are required to pass 2 cuts out of 3.

## 3.2 Conversion identification

### 3.2.1. The QPAIRF routine

The algorithm is based on the fact that, at the conversion point, the trajectories of both electrons are tangent. A loop is made on all electron pairs (as defined above) of opposite sign. The part of the helices that are parallel in the xy plane is identified. In each helix, the point where both tracks have the closest distance of approach if found. The middle of these points is defined as the conversion point. The following variables are defined:

- $d_{xy}$ (cm): distance in the xy-plane between the two helices at the closest approach to the conversion point.
- $d_z$ (cm) : z separation of the tracks at the closest approach to the conversion point.
- $m_{e+e-}$ (GeV) : invariant mass of the track pair (0 for a converted photon)
- $R_{mat}$ and $z_{mat}$ (cm): cylindrical coordinates of the interaction point.
- converted photon momentum, defined as the sum of the momenta of the tracks (the momentum transfer to the nucleus is neglected with a good approximation)

The following cuts (chosen in a range where MC reproduces the shape of data) are applied to select conversions :

$$m_{e+e-} < 15 \text{ MeV}$$

$$| d_{xy} | < 1 \text{ cm}$$

$$d_z < 2\text{cm}$$

As can be seen in fig. 2, the largest difference between MC and data lies in the invariant mass distribution. Therefore, in order to estimate the systematic error introduced by these cuts, the fraction

$$\frac{N_{conv}(15\text{MeV} < m_{e+e-} < 30\text{MeV})}{N_{conv}(0 < m_{e+e-} < 30\text{MeV})}$$

is compared between data and MC in a purified sample (taken between the ITC outer wall and the TPC inner wall where the background is low). The difference is 0.8% in the various data sets and will be taken as a systematic error.

### 3.2.2. Correction of the material simulation

Incorrectly simulated material leads to differences in the conversion probability between data and MC. The conversion probability distribution is computed for data and MC as a function of $R_{mat}$ by normalising the materialisation radius distributions to the number of conversions found in the TPC gas (45 cm < $R_{mat}$ < 100 cm* ) where the amount of material is known (after taking into account a known difference (11%) in the density of the gas between data and MC [1]).

The probability distributions are shown in fig. 3.a for data and MC and their ratio is shown in fig. 3.b for the inner region ($R_{mat}$ < 45 cm) and fig. 3.c for the TPC gas region. In the inner region, the simulation of material is not correct and the ratio shown in fig.3.b is used as a correction function for MC.

The statistical error on the number of conversions in the TPC is 1.2% (much larger than in the inner region) and will be taken as a systematic error on the final results. An additional error of 1% has to be accounted for, due to the uncertainty on the TPC gas pressure and temperature.

Then, a loose cut is applied on the materialisation radius: $R_{mat}$ > 3 cm as no photon can convert in this region (beam-pipe).

About 0.25 converted photon per event is accepted after these cuts, which leads to a total of about 500 000 conversions for the data (all statistics).

---

* This upper bound is set to avoid poorly reconstructed tracks.

## 3.3. Conversion purity and efficiency

Purity and efficiency are determined independently for data and MC, as a function of the track momentum. The ratio of efficiencies (data/MC) is then used as a correction function for MC.

### 3.3.1. Purity determination

The purity of the selection is determined independently for data and MC: for each track, the RI distribution is fitted with two gaussians by bins of $P_{track}$, and the contamination is then estimated by the fraction of track pairs passing the selection cuts and with at least one track belonging to the pion gaussian. This contamination is of the order of 1% in average and is corrected as a function of $P_{track}$ for both tracks.

### 3.3.2. RI, RT, RL efficiency

Differences between data and MC in the electron selection efficiency have to be estimated and corrected. The method is based on the assumption that, in a conversion pair, the estimators on one electron (1) are independent of the estimators on the associated electron (2). This assumption is valid at first order for low energy conversions, where the two tracks are well separated. Tight cuts are applied on track 1 and no cut on track 2; it produces a pure and unbiased track 2 sample. For this sample, the estimators distributions are fitted by bins of $P_{track2}$ to determine independently the efficiency on data and MC.

These efficiencies for the 3 data sets are shown in fig. 4.a-c-e for MC and data as a function of the momentum of the track 2 electron and their ratio is plotted in fig. 4.b-d-f: while 93' MC seems to reproduce correctly the 93' and 94' data, 92' MC shows a loss of efficiency at low momentum. This is due to the fact that the estimators are not equally centred and to differences in the number of hit wires in the TPC* .

The obtained ratio is then fitted and the resulting function will be used in the rest of the analysis as a weight (for each electron) to correct for the differences between data and MC.

Efficiency differences between data and MC have also been observed as a function of the transverse momentum (w.r.t. beam axis) of the tracks [2]. This behaviour is explained by a known effect in the MC, for tracks with several helix loops. It only affects very low energy tracks (Pt < 300 MeV) but an additional correction has to be applied as a function of the Pt of each track of the conversion (in the (Pt1,Pt2) plane) as they are correlated. This correction is estimated by the ratio data/MC of the (Pt1,Pt2) distributions, normalised to the number of converted pairs with Pt1 and Pt2 > 400 MeV.

---

* The hit wires are the wires used for the dE/dx calculation. The RI estimator is only defined if the number of hit wires is larger than 50.

# 4. Calibration of GAT efficiency

The GAT/converted photon invariant mass is computed for $E_{GAT} > 600$ MeV. Each converted photon in MC is weighted by the various correction functions computed in section 3, in order to correct for all differences of efficiencies between MC and data. Then the mass distributions are fitted by bins of $E_{GAT}$ for MC and data separately.

The total weight applied to the conversions in MC is the following:

$$W_{conv} = f_1(R_{mat}) \times f_2(P_{e-}) \times f_2(P_{e+}) \times f_3(Pt_{e-}, Pt_{e+})$$

with:

- $f_1$ : correction function on the material distribution (see 3.2.2)
- $f_2$ : correction function on the estimators efficiency (see 3.3.2.)
- $f_3$ : correction function on the Pt (see 3.3.2)

## 4.1. Fit of conversion/GAT invariant mass

The fit of the invariant mass distributions is performed with a third order polynomial for the background and two gaussians for the signal. As the number of parameter is too large to constraint the fit, the ratio of the parameters (mean and width) of the two gaussians is previously determined from MC and parametrised. An example of fit is given in fig.5.a (bin $0.04<x_{GAT}<0.05$)

The $\chi^2$/ndf of the fits are shown in fig. 5.c for data and 5.d for MC for the various bins of $x_{GAT}$ and the ratios of the fitted number of $\pi^0$'s in MC over the number of matched* $\pi^0$'s are shown in fig. 5.b. These ratios are compatible with 1 within the statistical errors.

## 4.2. Calibration procedure

In order to compute the relative efficiencies between data and MC for GAT reconstruction, the fitted number of $\pi^0$'s in each bin of $E_{GAT}$ must be normalised so that a possible difference resulting from the physics processes would not appear in the comparison. The assumption is made that the data and MC efficiency are the same for all GAT's of energy larger than 3 GeV. This assumption is based on results from $\tau$ decays [3] showing that for photons of energy greater than 3 GeV, the gamma/gamma invariant mass spectrum is perfectly reproduced by MC. A second

---

* The "matched" $\pi^0$ are the reconstructed $\pi^0$'s that are matched to the corresponding generated track in the MC
The matching procedure is done in the following way:

- charged tracks are matched using the ALPHA routine KBESTM
- GAT's are matched by looking at generated photons belonging to the same ECAL cluster and resolving any ambiguity by an angular matching.

argument in favour of this assumption is the fact that the fitted mass and width of the $\pi^0$ reconstructed from two GAT's of energy larger than 3 GeV (see 6.1. and fig. 13.a) is also perfectly reproduced by MC. The normalisation factor is then defined as the number of $\pi^0$'s with a GAT of energy greater than 3 GeV. This factors is determined with a statistical error, that will be taken into account as a systematic error in the final result. In addition, at 3 GeV, the energy calibration error is estimated to be 2% (which means that what one calls 3 GeV could be 3.06 GeV). This leads to a systematic error of 2.5% on the number of $\pi^0$'s with $E_{GAT} > 3$ GeV.

Then, one has:

$$\frac{N_{\pi^0}(E_{GAT})_{data} \,/\, N_{\pi^0}(E_{GAT} > 3GeV)_{data}}{N_{\pi^0}(E_{GAT})_{mc} \,/\, N_{\pi^0}(E_{GAT} > 3GeV)_{mc}} = \frac{\varepsilon_{GAT}(E_{GAT})_{data}}{\varepsilon_{GAT}(E_{GAT})_{mc}} = W_{GAT}(E_{GAT})$$

the ratio $W_{GAT}$ as a function of $x_{GAT}$ is shown in fig. 6. A loss of efficiency in data is seen at low $x_{GAT}$, with a larger effect in 94, where MC was not tuned for the data. This ratio is parametrised and applied as a weight to each MC GAT.

The normalisation also assumes that the generator reproduces correctly the shape of the $\pi^0$ energy distribution. But the final result (fig. 9.b) shows that the ratio data/MC of the $\pi^0$ energy distributions is not flat. The slope of this ratio is then fitted and applied to MC events as a weight in order to recompute the $W_{GAT}$ function. This is equivalent to a change in the shape of the generated $\pi^0$ energy spectrum. The whole induced change in the final result is quoted as the systematic error (2.4% for the 3 data sets combined).

# 5. Inclusive $\pi^0$ spectra from GAT/conversion pairs

Conversion/GAT invariant mass distributions are fitted and the resulting signal/noise rate will be used to correct data and MC independently.

The total weight applied to any conversion/GAT pair in MC is :

$$W_{tot} = W_{conv} \times W_{GAT}$$

## 5.1. Fit of conversion/GAT invariant mass

The signal/noise rate, mainly sensitive to the $\pi^0$ energy, shows also a dependence on the angle between the $\pi^0$ and the thrust axis: a $\pi^0$ located in the centre of the jet, will be surrounded by a larger number of particles, resulting in an increased background. The signal/noise rate has therefore been parametrised as a function of both the $\pi^0$ energy and the angle ($\theta$) with the thrust axis.

The invariant mass distribution has been plotted into 12 bins of $x_{\pi}{}^0$ and 4 bins of $\theta$. The following cuts have been applied:

$$x_{\pi 0} > 0.025$$

$$\left| \frac{E_{conv} - E_{GAT}}{E_{\pi^0} - 600\ \text{MeV}} \right| < 0.8$$

The last cut has been set to avoid very asymmetric photon pairs that would increase the background.

The signal and background are fitted as in 4.1. The result for the fitted mass and width is shown in fig. 7.a-b.

## 5.2. Signal / noise determination

The signal/noise rate is determined in the following mass range (representing about two sigmas around the peak mean value):

$$100\ \text{MeV} < m_{GAT/conv} < 170\ \text{MeV}$$

and is shown in fig. 8.b. A parametrisation of these results (the lines in fig.8.b) is used as a weight in the final $\xi = -\ln(x_{\pi}{}^0/x_{beam})$, Pt and rapidity distributions.

## 5.3. Efficiency correction

The global efficiency correction can be computed independently for the three distributions and a bin by bin correction is applied, using the following correction procedure:

$$(\text{data corr.})_i = (\text{data})_i \times \frac{(\text{MC "true"})_i}{(\text{MC weighted by } W_{tot})_i}$$

where i represents a bin in any distribution $\xi$, Pt or Y, and the weight $W_{tot}$ is defined at the beginning of this chapter. The MC "true" distributions correspond to hadron level $\pi^0$'s (FKIN) giving at least one "observable" (KSTABC = 1,2,-3) descendant in fully processed MC events. This definition gives a $\pi^0$ rate and energy spectrum identical (within statistical errors) to the one obtained at generator level (KINGAL only with max. decay time set to 1nsec).

The MC distributions are weighted so that the ratio

$$\frac{(\text{MC weighted by } W_{tot})_i}{(\text{MC "true"})_i}$$

represents the global* efficiency for the data. This efficiency is shown in fig. 8.a as a function of $x_{\pi^0}$ (full circles). The MC efficiency (computed without weighting by $W_{tot}$) is also shown (open circles).

* this efficiency is called global because it's an average (by bins of $x_{\pi^0}$) of different factors: conversion rate, track reconstruction efficiency, conversion identification efficiency and GAT reconstruction efficiency.

## 5.4 Systematics

The systematic errors have been evaluated in the following way for the different parts of the analysis.

### 5.4.1 Conversion selection

• QPAIRF : the fraction of conversions for which $m_{e+e-} > 15$ MeV has been compared between data and MC and the difference, 0.8% , has been taken as the systematic error for the 3 data sets. (see 3.2.1.)

• Material simulation correction: the error is the quadratic sum of the statistical error on the normalisation in the TPC gas (1.2%) and of the TPC pressure uncertainty (1%). (3.2.2.)

• Electron estimators correction: the fit of the correction function has been varied by $\pm$ 1 $\sigma$ where $\sigma$ represents the statistical error on the fitted points (3.3.2.)

• Background estimation: the background correction being very small (1%), the error on its estimation is negligible. (3.3.1.)

• Track Pt correction: for each bin in the ($Pt_1$,$Pt_2$) plane (see 3.2.2.), the value of the correction has been varied randomly with a gaussian shape, the $\sigma$ of the gaussian being the error on the correction value. The experiment has been repeated 100 times giving for each bin of the measured distributions ($\xi$, Pt, Y) a gaussian distribution centred on the result in the bin. The width of this gaussian has been taken as the systematic error.

### 5.4.2. GAT photon

• calibration of the GAT efficiency: the statistical error on the normalisation factor (number of $\pi^0$'s with $E_{GAT} > 3$ GeV) is 1.5% for the combined result. of the 3 data sets (4.2.).

• Uncertainty on the calibration of the GAT energy: the error on the calibration itself is 2%, resulting in a 2.5% error on the normalisation factor.

• As mentioned in 4.2., an extra systematic error had to be added, resulting from the $\pi^0$ energy dependence of the ratio (data corr./gen.), which was not taken into account in the normalisation of the efficiencies. This error is 2.4% for the combined result.

### 5.4.3. $\pi^0$ signal extraction

• signal/noise rate in the data: the fit of the correction function has been varied by $\pm$ 1 $\sigma$ where $\sigma$ represents the statistical error on the fitted points (5.2.)

• global efficiency correction (MC statistics): the dominant error comes from the determination of the MC signal/noise rate and is therefore estimated in the same way it was done for the data.

A summary of the errors for the 3 data sets and for the combined results (each year has been weighted with its statistics) is given in table 1.

| | effic. estim. | correc. Pt | $R_{mat}$ | cut $M_{e+e-}$ | norm. GAT | calibr. ECAL | slope data/mc | S/B (data) | MC stat. | TOTAL |
|---|---|---|---|---|---|---|---|---|---|---|
| 92 | 1.3 | 0.4 | 1.6 | 0.8 | 3.0 | 2.5 | 4.4 | 4.7 | 5.3 | 9.5 |
| 93 | 1.2 | 0.4 | | | 2.8 | | 4.2 | 4.1 | 4.1 | 8.4 |
| 94 | 1.2 | 0.3 | | | 2.3 | | 3.8 | 3.4 | 4.0 | 7.6 |
| comb. | 0.9 | 0.2 | 1.6 | 0.8 | 1.5 | 2.5 | 2.4 | 2.3 | 2.6 | 5.5 |

table 1 (all numbers are in %)

## 5.5 Results

The $\xi$, Pt and rapidity distributions (3 data sets combined) are given on fig. 9, 10, 11 and in tables 4, 5, 6. They are compared to HVFL04. The $\xi$ spectrum is plotted with statistical and systematic errors added in quadrature; the Pt and rapidity spectra are plotted with statistical errors only.

The integrated number of $\pi^0$'s , computed on the range $0.025 < x_{\pi^0} < 1$ is given in table 2, for the 3 data sets and the combined result in table 3, as well as the extrapolation to the whole range from both generators.

| | $N_{\pi^0}$ (x = 0.025 to x = 1.) |
|---|---|
| 92 | 5.28 ± 0.03 ± 0.50 |
| 93 | 5.25 ± 0.03 ± 0.44 |
| 94 | 5.21 ± 0.02 ± 0.40 |

table 2 (the first error is statistic, the second systematic)

| | data (92-93-94 comb.) | HVFL04 |
|---|---|---|
| $N(\pi^0)$ x = 0.025 to 1. | 5.24 ± 0.02 ± 0.29 | 4.68 |
| $N(\pi^0)$ x = 0. to 1. | 10.51 ± 0.03 ± 0.58 | 9.39 |

table 3 (the first error is statistic, the second systematic)

| $\xi_{\pi^0}$ bin | $1/\sigma_{had}\ d\sigma_{had}/dx$ | stat. err. | syst. err. | HVFL04 |
|---|---|---|---|---|
| .2 - .4 | .017 | .001 | .001 | .018 |
| .4 - .5 | .034 | .002 | .001 | .039 |
| .5 - .6 | .055 | .002 | .002 | .060 |
| .6 - .7 | .085 | .003 | .003 | .089 |
| .7 - .8 | .115 | .003 | .004 | .125 |
| .8 - .9 | .162 | .004 | .006 | .166 |
| .9 - 1.0 | .219 | .005 | .008 | .214 |
| 1.0 - 1.1 | .272 | .005 | .010 | .278 |
| 1.1 - 1.2 | .323 | .005 | .012 | .339 |
| 1.2 - 1.3 | .415 | .006 | .015 | .416 |
| 1.3 - 1.4 | .505 | .007 | .019 | .501 |
| 1.4 - 1.5 | .623 | .007 | .024 | .593 |
| 1.5 - 1.6 | .710 | .008 | .028 | .696 |
| 1.6 - 1.7 | .828 | .008 | .033 | .805 |
| 1.7 - 1.8 | .937 | .009 | .038 | .915 |
| 1.8 - 1.9 | 1.102 | .010 | .045 | 1.049 |
| 1.9 - 2.1 | 1.309 | .007 | .050 | 1.237 |
| 2.1 - 2.3 | 1.614 | .008 | .064 | 1.508 |
| 2.3 - 2.5 | 1.913 | .009 | .079 | 1.781 |
| 2.5 - 2.7 | 2.253 | .011 | .097 | 2.054 |
| 2.7 - 2.9 | 2.619 | .013 | .118 | 2.324 |
| 2.9 - 3.1 | 2.923 | .016 | .140 | 2.601 |
| 3.1 - 3.3 | 3.190 | .020 | .163 | 2.823 |
| 3.3 - 3.5 | 3.568 | .032 | .197 | 2.996 |
| 3.5 - 3.7 | 3.799 | .064 | .229 | 3.108 |

table 4

| $Pt_p{}^0$bin(GeV) | $1/s_{had}\ ds_{had}/dPt$ | stat. err. | syst. err. | HVFL04 |
|---|---|---|---|---|
| .0 - .1 | 10.730 | .084 | .912 | 9.070 |
| .1 - .2 | 19.325 | .095 | 1.288 | 16.737 |
| .2 - .3 | 17.473 | .080 | 1.057 | 15.681 |
| .3 - .4 | 13.607 | .065 | .740 | 12.452 |
| .4 - .5 | 10.232 | .053 | .513 | 9.334 |
| .5 - .7 | 6.198 | .027 | .256 | 5.931 |
| .7 - .9 | 3.320 | .019 | .133 | 3.203 |
| .9 - 1.1 | 1.919 | .013 | .076 | 1.845 |
| 1.1 - 1.3 | 1.211 | .010 | .048 | 1.150 |
| 1.3 - 1.5 | .842 | .008 | .033 | .766 |
| 1.5 - 1.8 | .520 | .005 | .020 | .494 |
| 1.8 - 2.1 | .315 | .004 | .012 | .308 |
| 2.1 - 2.4 | .217 | .003 | .008 | .203 |
| 2.4 - 2.7 | .149 | .002 | .006 | .137 |
| 2.7 - 3.0 | .096 | .002 | .004 | .097 |
| 3.0 - 3.5 | .069 | .001 | .002 | .064 |
| 3.5 - 4.0 | .042 | .001 | .002 | .040 |
| 4.0 - 4.5 | .027 | .001 | .001 | .026 |
| 4.5 - 5.0 | .018 | .001 | .001 | .017 |
| 5.0 - 6.7 | .0086 | .0003 | .0003 | .0079 |
| 6.7 - 8.3 | .0025 | .0001 | .0001 | .0026 |
| 8.3 - 10.1 | .0011 | .0001 | .0001 | .0010 |

table 5.

| $Y_{\pi^0}$bin(GeV) | $1/\sigma_{had}\ d\sigma_{had}/dY$ | stat. err. | syst. err. | HVFL04 |
|---|---|---|---|---|
| .0 - .4 | 3.375 | .064 | .130 | 2.729 |
| .4 - .8 | 3.494 | .042 | .140 | 2.988 |
| .8 - 1.2 | 3.264 | .032 | .138 | 3.054 |
| 1.2 - 1.5 | 3.167 | .029 | .145 | 3.035 |
| 1.5 - 1.8 | 3.085 | .024 | .140 | 2.967 |
| 1.8 - 2.1 | 2.953 | .019 | .131 | 2.842 |
| 2.1 - 2.3 | 2.897 | .019 | .147 | 2.682 |
| 2.3 - 2.5 | 2.771 | .017 | .144 | 2.494 |
| 2.5 - 2.7 | 2.537 | .014 | .126 | 2.267 |
| 2.7 - 2.9 | 2.146 | .012 | .113 | 1.988 |
| 2.9 - 3.1 | 1.857 | .010 | .100 | 1.689 |
| 3.1 - 3.3 | 1.498 | .009 | .077 | 1.369 |
| 3.3 - 3.5 | 1.168 | .007 | .055 | 1.076 |
| 3.5 - 3.7 | .847 | .006 | .038 | .805 |
| 3.7 - 3.9 | .613 | .005 | .029 | .584 |
| 3.9 - 4.1 | .417 | .004 | .019 | .404 |
| 4.1 - 4.6 | .208 | .002 | .008 | .205 |
| 4.6 - 5.1 | .060 | .001 | .002 | .059 |
| 5.1 - 6.5 | .0056 | .0003 | .0002 | .0051 |

table 6.

# 6. Inclusive $\pi^0$ spectrum from two GAT photons

The invariant mass is computed from two GAT's, and the total correction weight applied to the MC GAT in order to compute the data efficiency is defined by :

$$W_{GAT1} \times W_{GAT2} = f(E_{GAT1}) \times f(E_{GAT2})$$

where f is the calibration function defined in 4.2.

## 6.1. Fit of GAT/GAT invariant mass

The signal peak (see. fig. 12.a) is wider (as expected) than in the GAT/conv case (20 to 30 MeV). Therefore, the fitting function has to be more constrained. Compared to the GAT/conv case (see 4.1), the ratio of the two signal gaussians is fixed to 20% and the background function is a second order polynomial. In this analysis, the invariant mass has only been plotted by bins of $x_{\pi^0}$.

At low energy, the signal peak becomes too wide to be fitted. This region is removed with $x_{\pi^0}>0.04$. At high energy, a cut ($x_{\pi^0} < 0.5$, removes 1% of the total) is needed to remove unfitable mass distribution.

An example of the fit is given in fig. 12.a, the $\chi^2$/ndf is shown in fig. 12.c for data and 12.d for MC and the ratio fitted/matched in fig. 12.b.: the $\chi^2$/ndf values are larger than 1 for some points and the fitted/matched ratios are not always compatible with 1, as a result of the stronger constraint on the fit function. Therefore an extra systematic error was assigned: half difference between the points further apart in the fitted/matched ratio (taking into account their statistical significance). This error is 2.5%.

The fitted mass and width are shown in fig. 13.a-b as a function of $x_{\pi^0}$. The mass increases at high energy: when both photons from the $\pi^0$ are close in angle, the reconstruction tends to overestimate the energy for each GAT.

## 6.2. Signal / background determination and efficiency correction

The dependence of the fitted mass and width on the $\pi^0$ energy are parametrised in order to optimise the signal/noise. The mass window is set to [- 2$\sigma$ ; + 1.5$\sigma$]. The asymmetry of the window is due to the asymmetric shape of the background under the peak. The signal/noise rate is shown in fig. 13.c and appears to be higher in MC than in data by a few percent. This rate is parametrised and used to correct the $\xi$ distribution.

The global efficiency (fig. 13.d, full circles) is, as above, computed from MC weighted by the calibration function in order to reproduce correctly the data. The efficiency for MC (no weight) is shown on the same figure with open circles.

## 6.3 Systematics

### 6.3.1. GAT photons

• calibration of the GAT efficiency: the systematics are the same as in the conversion/GAT case because the calibration function is the same. But they have to be multiplied by $\sqrt{2}$ as the calibration function is used for both GAT's.

### 6.3.2. $\pi^0$ signal extraction

• invariant mass fitting procedure: half distance between the extreme points in the fitted/matched ratio (2.5%)
• signal/noise correction: same procedure as in the GAT/conv analysis
• global efficiency correction (MC stat): same procedure as in the GAT/conv analysis

The summary of systematics is shown in table 7. for the 3 data sets, as well as for the combined result.

| | norm. GAT | calibr. ECAL | slope data/mc | fit | S/B (data) | MC stat. | TOTAL |
|---|---|---|---|---|---|---|---|
| 92 | 4.2 | | 4.2 | | 2.4 | 3.7 | 8.6 |
| 93 | 4.0 | 3.5 | 4.0 | 2.5 | 2.4 | 2.7 | 6.0 |
| 94 | 3.3 | | 3.6 | | 1.3 | 2.4 | 7.1 |
| comb. | 2.2 | 3.5 | 2.3 | 2.5 | 1.1 | 1.7 | 5.7 |

table 7 (all numbers are in %)

Out of these 5.7%, 3.7% are common to the conv/GAT analysis and 4.2% are independant.

### 6.4 Results

The resulting $\xi$ distribution is shown in fig. 14 with statistical errors only. It shows a very similar behaviour to the distribution obtained in the conversion/GAT study.

The integrated result between $x_{\pi^0} = 0.04$ and $x_{\pi^0} = 0.5$ is shown in table 8 for the 3 data sets and in table 9 for the combined result and its extrapolation to the whole energy range. In both tables, the results are compared to the result given by the conversion/GAT study in the same integration range.

| | data (GAT/GAT) | data (GAT/conv) |
|---|---|---|
| 92 | $3.59 \pm 0.004 \pm 0.31$ | $3.59 \pm 0.01 \pm 0.34$ |
| 93 | $3.53 \pm 0.004 \pm 0.28$ | $3.51 \pm 0.01 \pm 0.29$ |
| 94 | $3.69 \pm 0.003 \pm 0.26$ | $3.54 \pm 0.01 \pm 0.27$ |

table 8 (the first error is statistic, the second systematic)

| | data (GAT/GAT) | data (GAT/conv) | HVFL04 |
|---|---|---|---|
| $N(\pi^0)$ x =0.04 to 0.5 | $3.63 \pm 0.007 \pm 0.21$ | $3.56 \pm 0.02 \pm 0.20$ | 3.26 |
| $N(\pi^0)$ x = 0. to 1. | $10.46 \pm 0.02 \pm 0.60$ | $10.25 \pm 0.06 \pm 0.58$ | 9.39 |

table 9 (the first error is statistic, the second systematic)

# 7. Conclusions

A method combining converted photons and ECAL photons has been developed to measure the inclusive $\pi^0$ production in hadronic decays of the $Z^0$. Sources of differences between data and MC efficiencies have been studied and corrected: low Pt track reconstruction, electron identification, conversion selection and ECAL photon reconstruction.

The total number of $\pi^0$ per event is measured to be $5.24 \pm 0.02$ (stat.) $\pm 0.029$ (syst.) in the $x_{\pi^0}$ range [0.025;1]. It shows a slight discrepancy (two sigmas) with HVFL04 . This result is compatible (within errors) with the results presented in another analysis [4].

As a check, this analysis was extended to combinations of two ECAL photons. The results of both analysis show a good agreement, in the total numbers of $\pi^0$ as well as in the $\xi$ distributions.

# References:

[1] Measurement of the inclusive photon spectrum using e+e- conversions - F. Stephan - ALEPH 95-015

[2] 1993 TPC selection - A. Lucotte - ALEPH 94-170

[3] Performances of the ALEPH detector at LEP - CERN preprint PPE/94-170

[4] Measurement of the inclusive $\pi^0$ spectrum with the ALEPH detector - P. van Gemmeren - ALEPH 95-041

# Note for figures:

93 data set: fig. 1,2,5,7,8,12,13

combined (92+93+94) data sets: 3,9,10,11,14

# fig. 1: electron estimators - fig. 2.: conversion variables

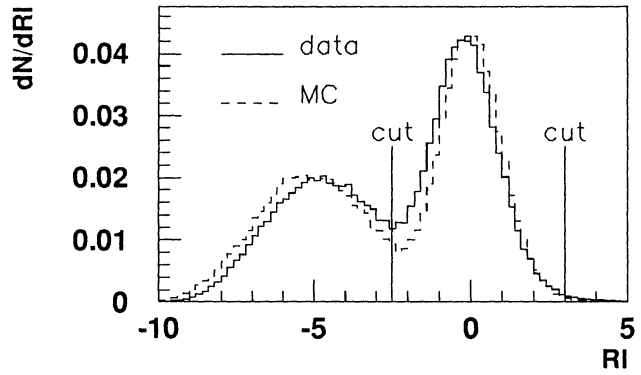


fig. 1.a

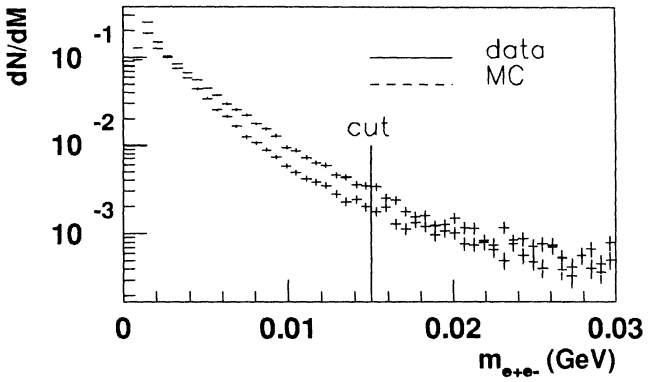


fig. 2.a

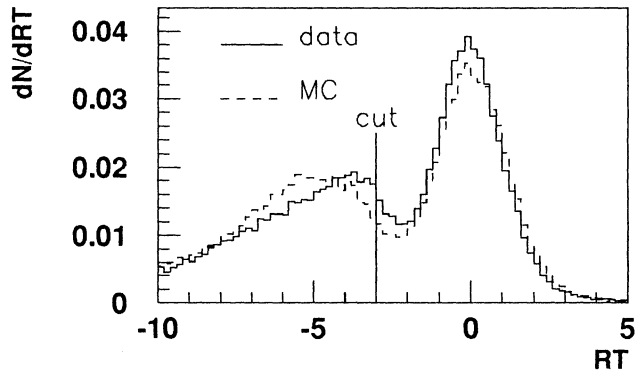


fig. 1.b

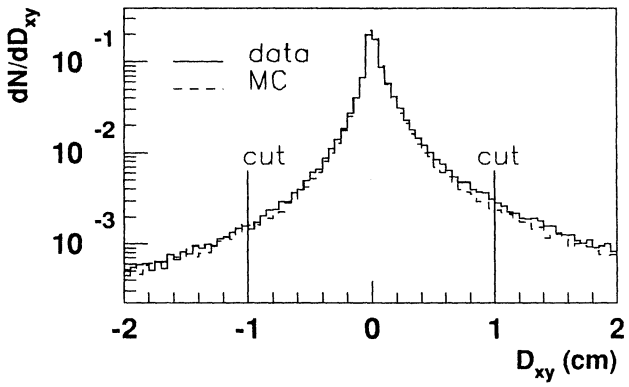


fig. 2.b

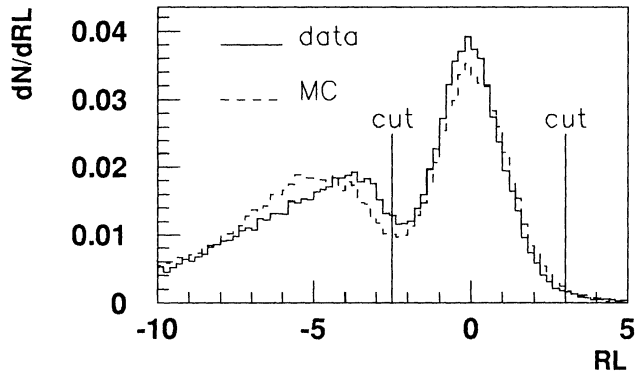


fig. 1.c

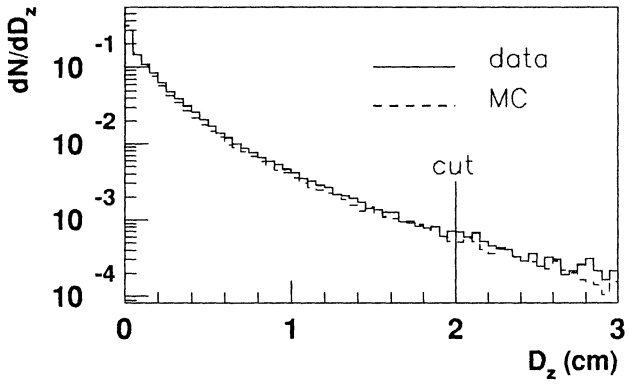


fig. 2.c

# fig. 3

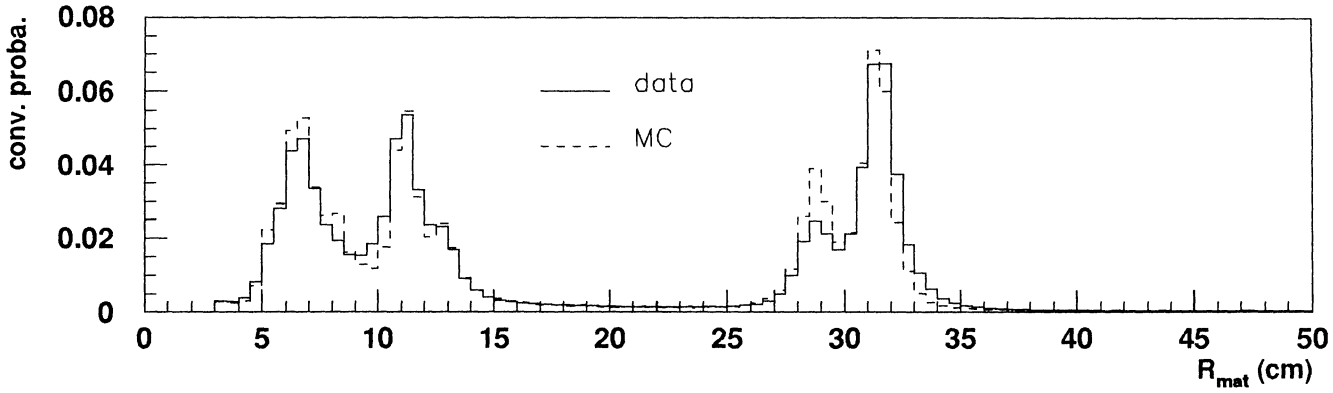


fig. 3.a: conversion probability density

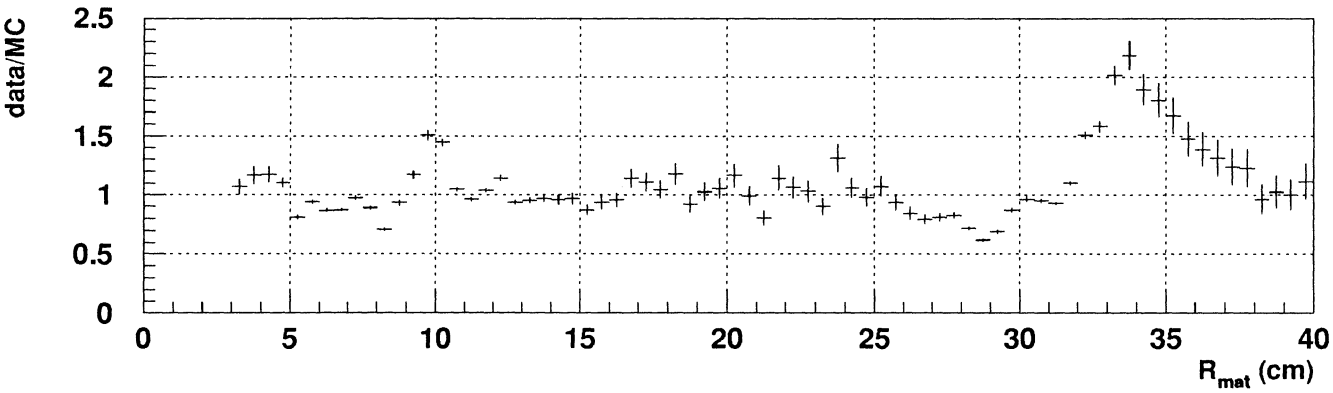


fig. 3.b: ratio of probability data/MC (inner region)

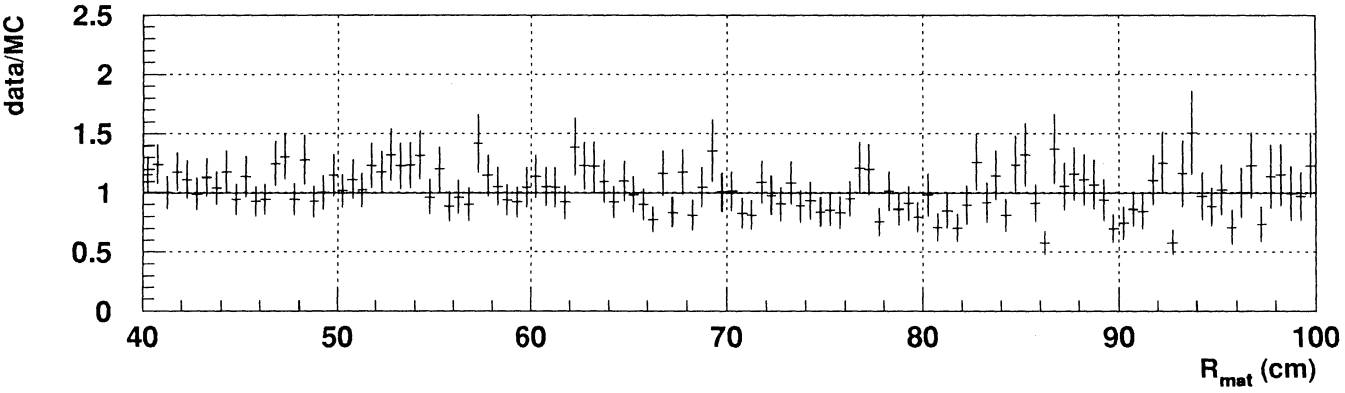


fig. 3.c: ratio of probability data/MC (TPC gas region)

# fig. 4: electron estimators efficiency

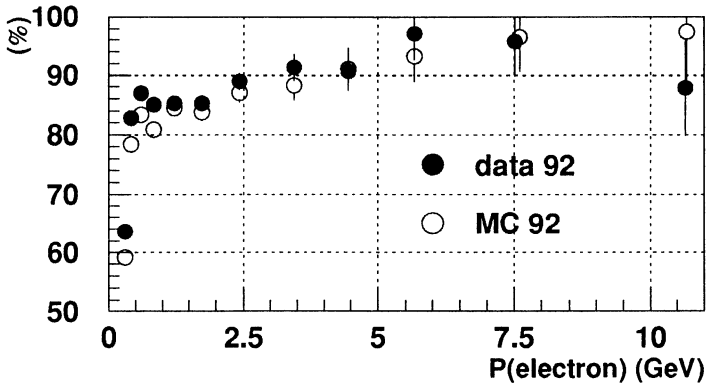


fig. 4.a: 92

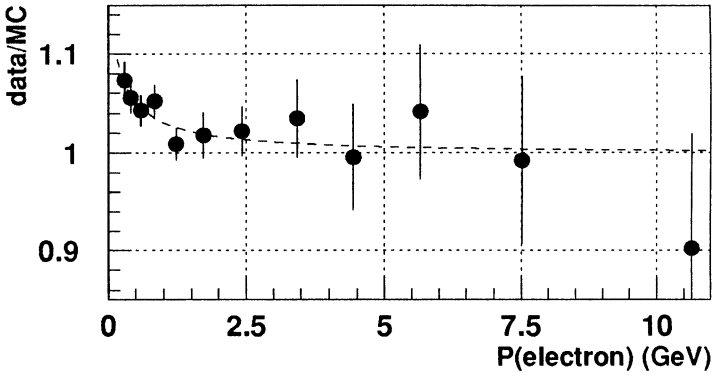


fig. 4.b: 92 (ratio data/MC)

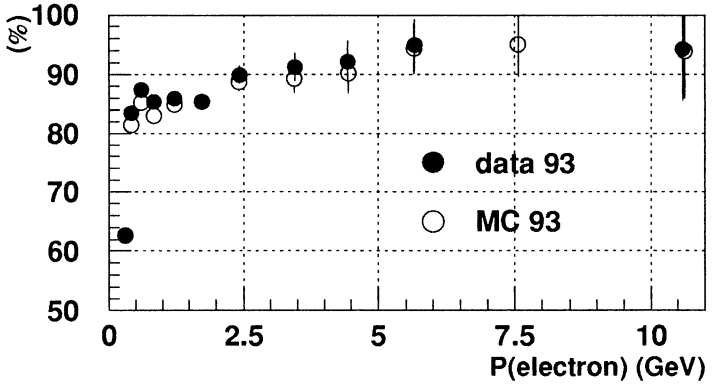


fig. 4.c: 93

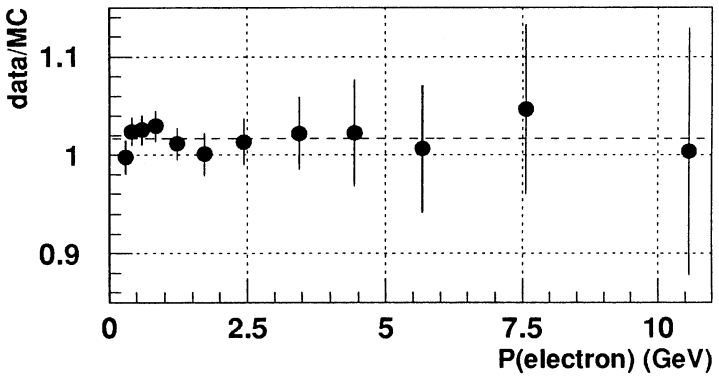


fig. 4.d: 93 (ratio data/MC)

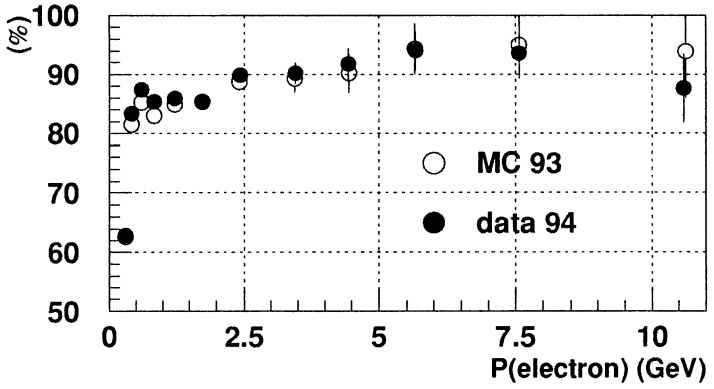


fig. 4.e: 94

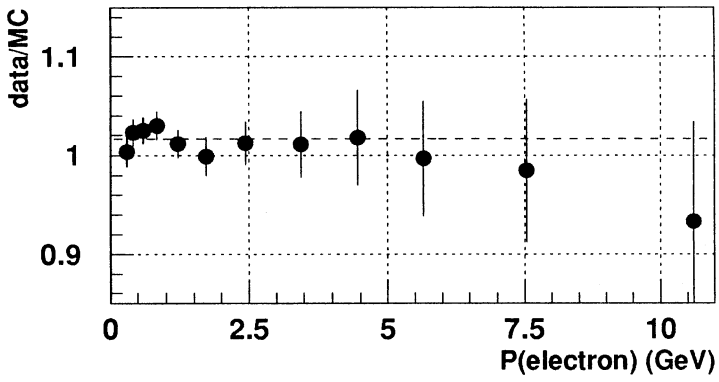


fig. 4.f: 94 (ratio data/MC)

# fig. 5: fit results ($x_{GAT}$ bins)

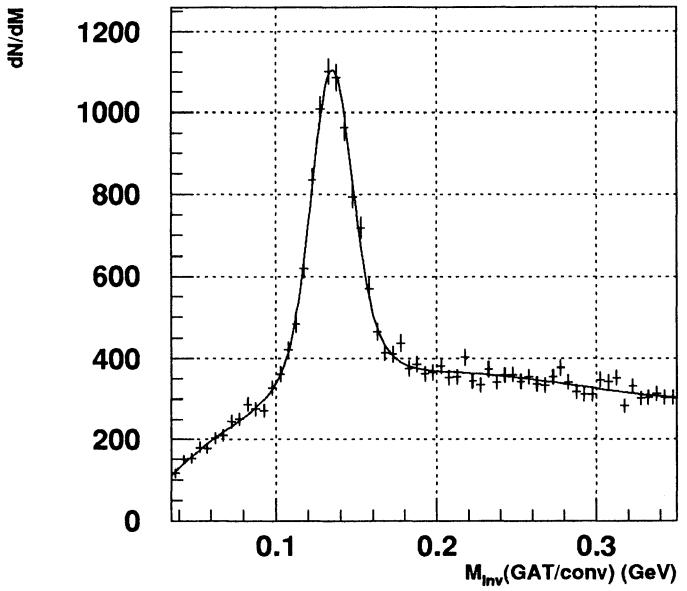


fig. 5.a: $0.04<x_{GAT}<0.05$

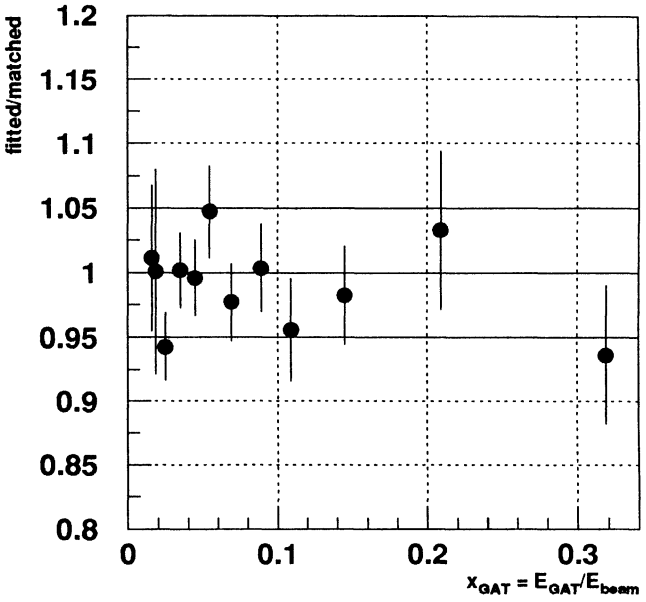


fig. 5.b: fitted/matched ratio

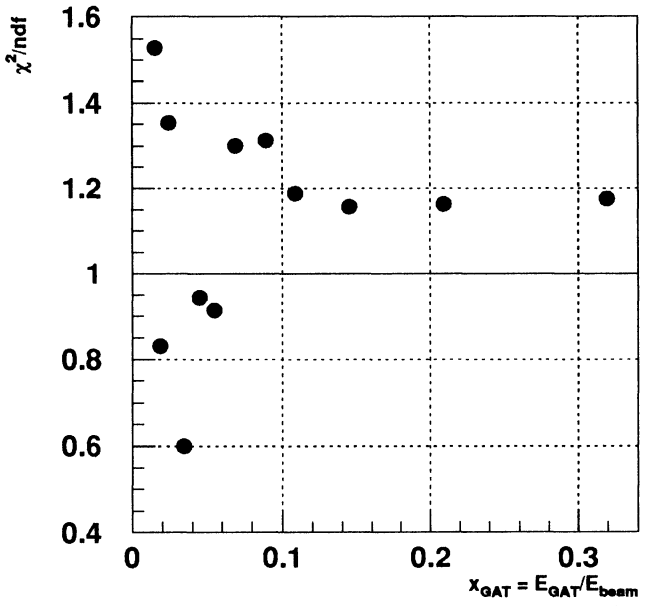


fig. 5.c: $\chi^2$/ndf data

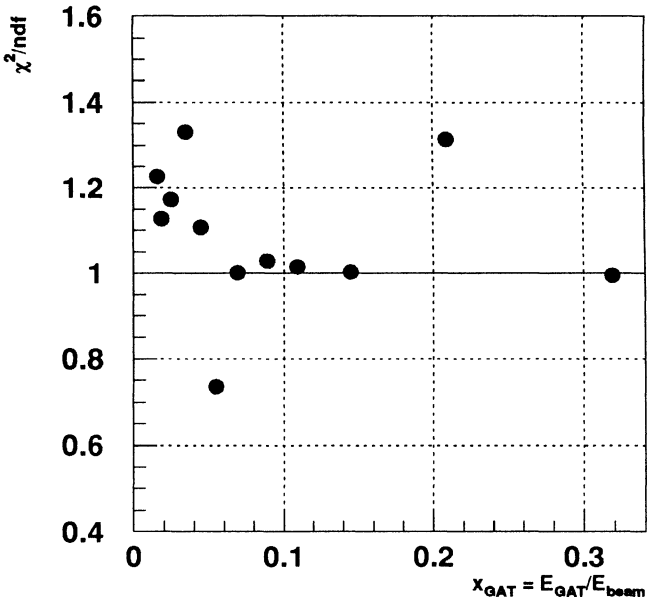


fig. 5.d: $\chi^2$/ndf MC

# fig. 6: efficiencies of GAT (data/MC)

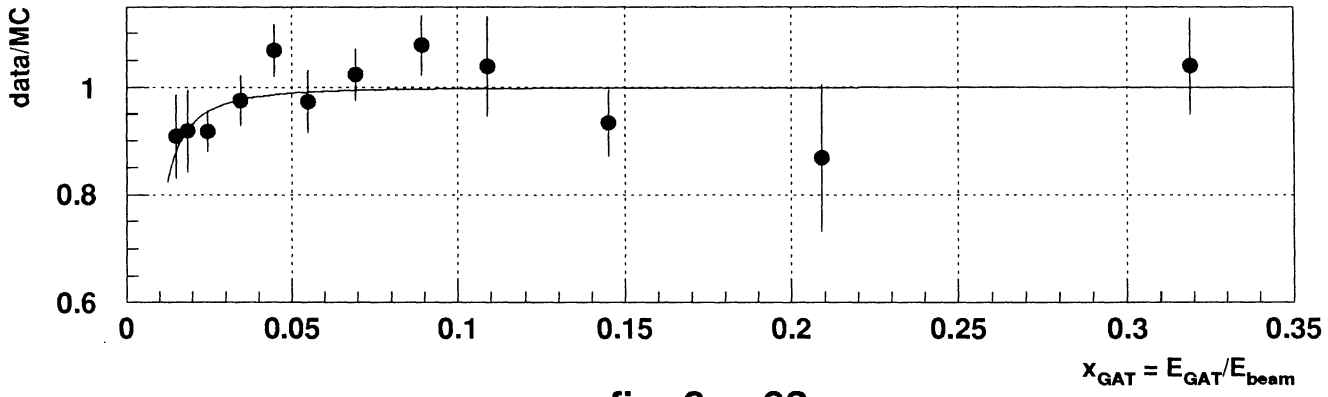


fig. 6.a: 92

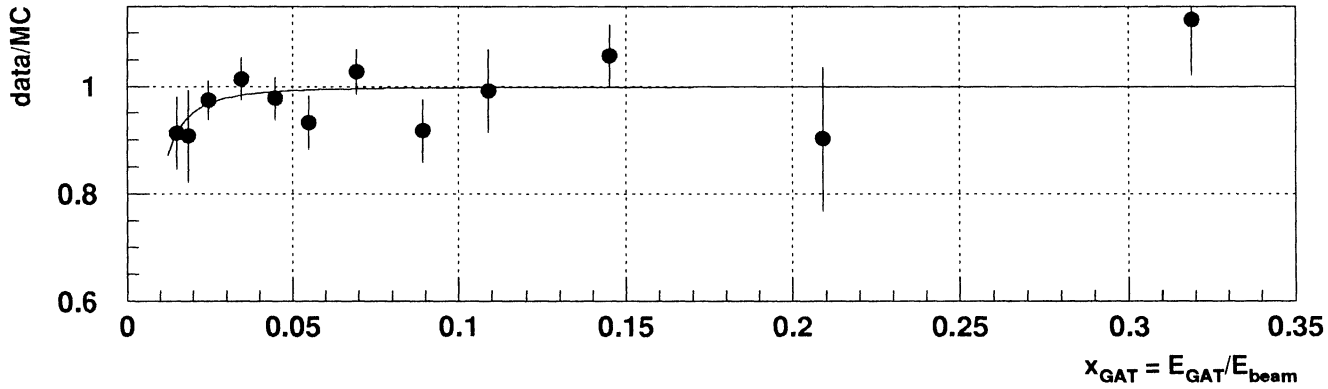


fig. 6.b: 93

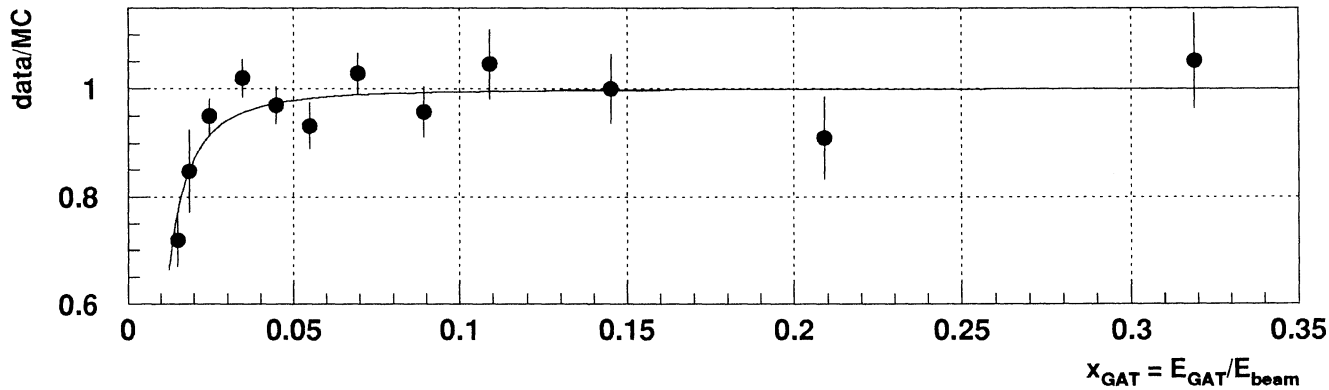


fig. 6.c: 94

# fig. 7: $\pi^0$ fitted mass and width

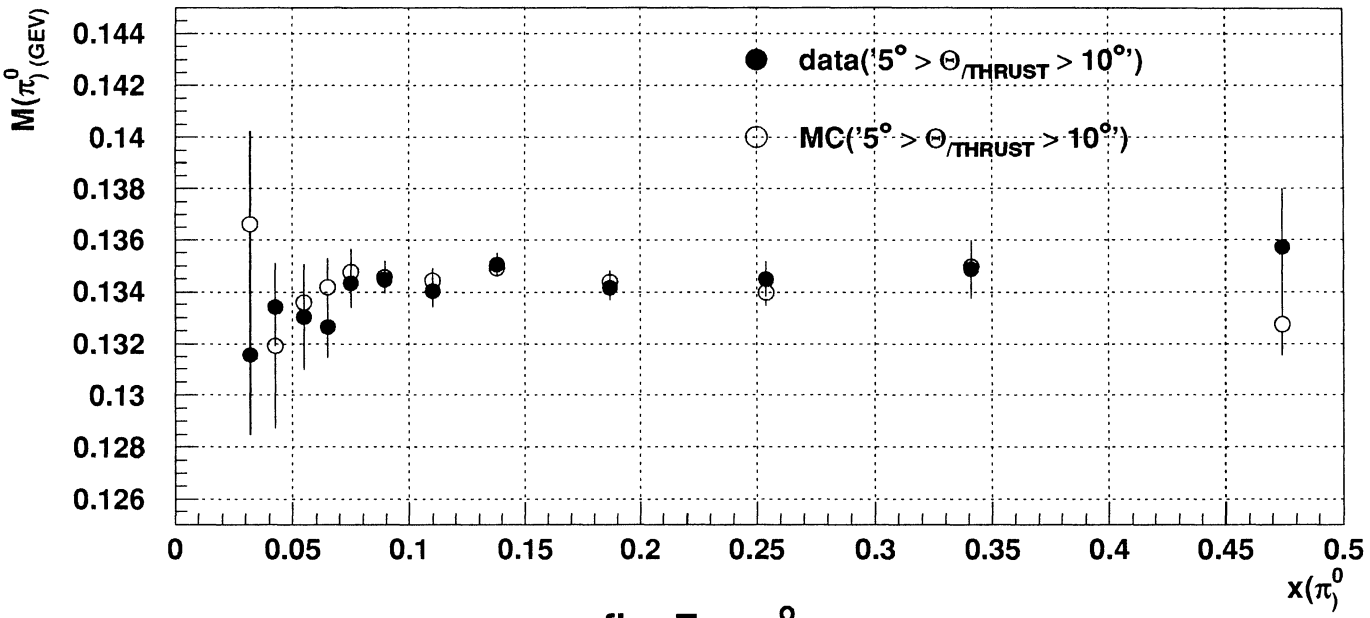


fig. 7.a: $\pi^o$ mass

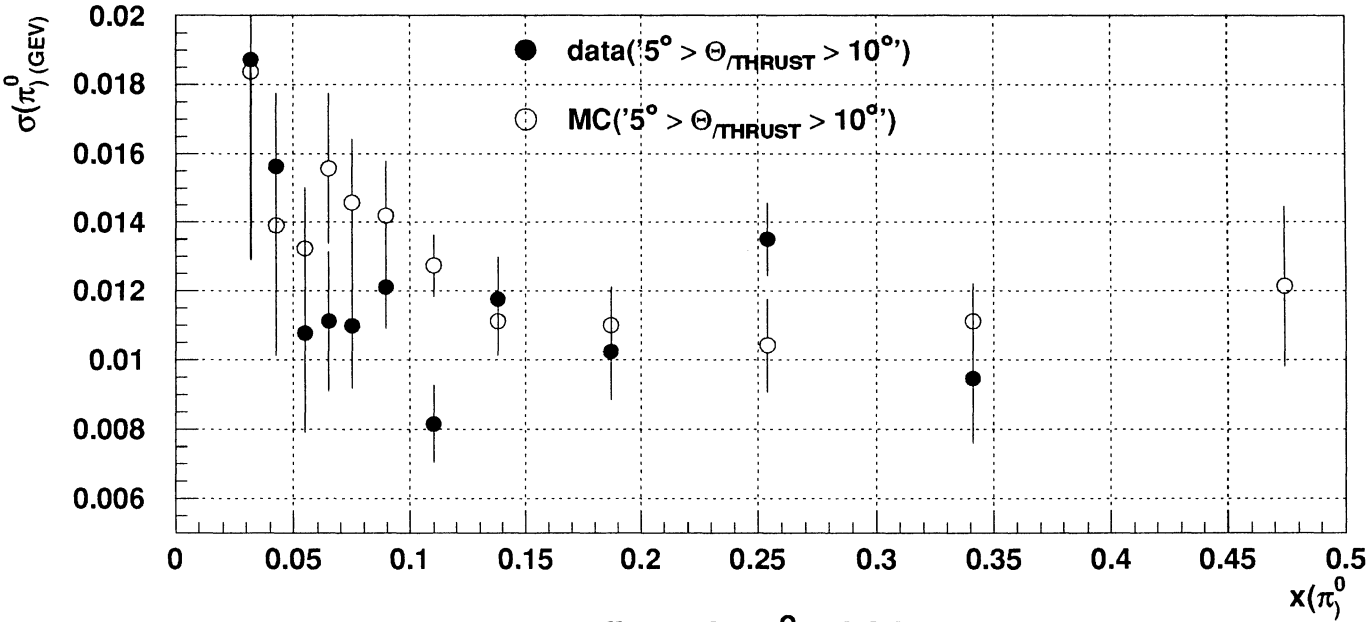


fig. 7.b: $\pi^o$ width

# fig. 8: global efficiency and (signal/signal+noise) rate

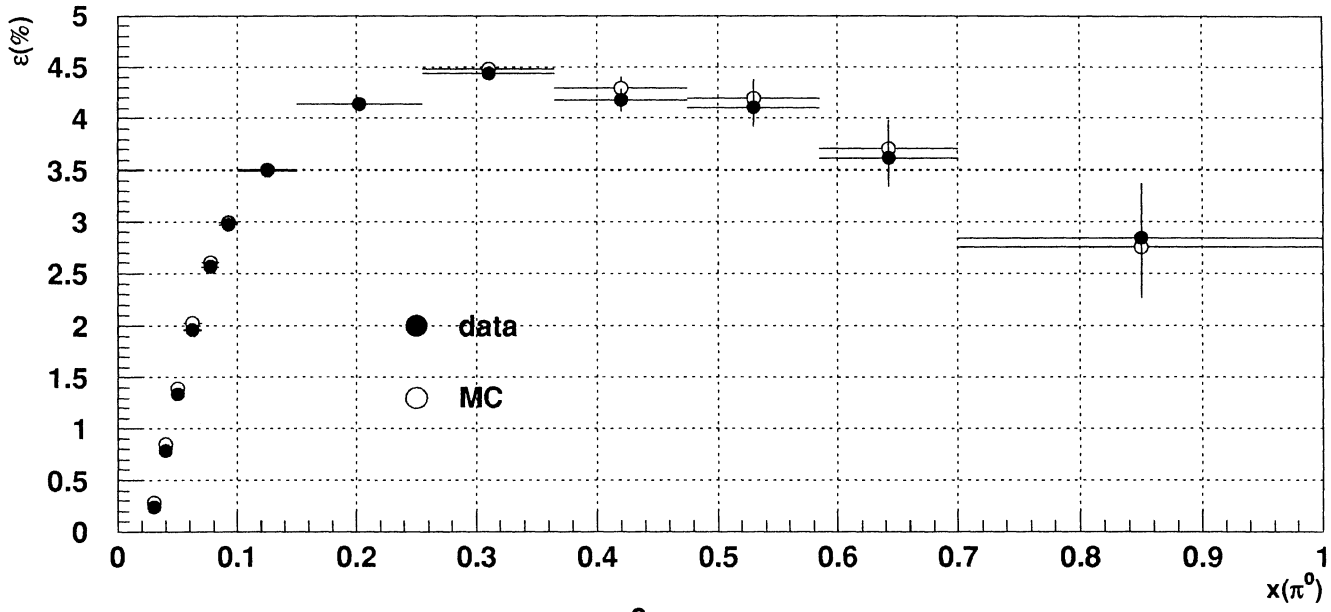


fig. 8.a: $\pi^0$ global efficiency

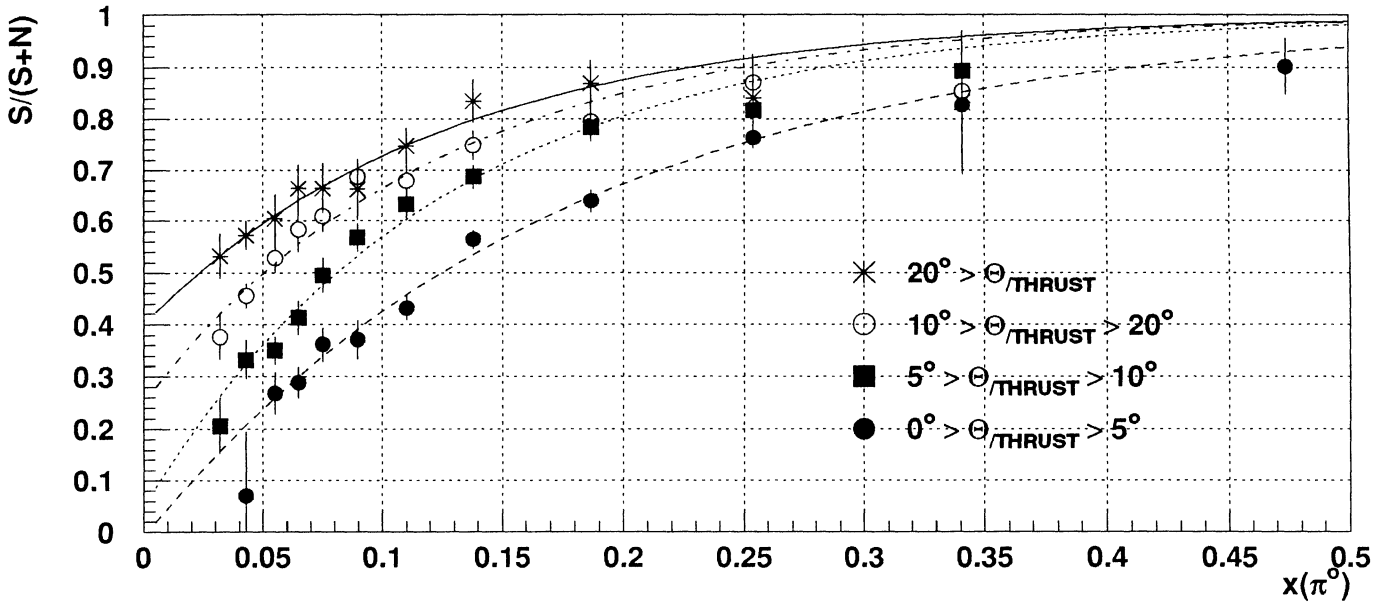


fig. 8.b: signal/(signal+noise) rate (data)

# fig. 9: $\pi^o$ $\xi$ spectrum (stat.+syst. errors)

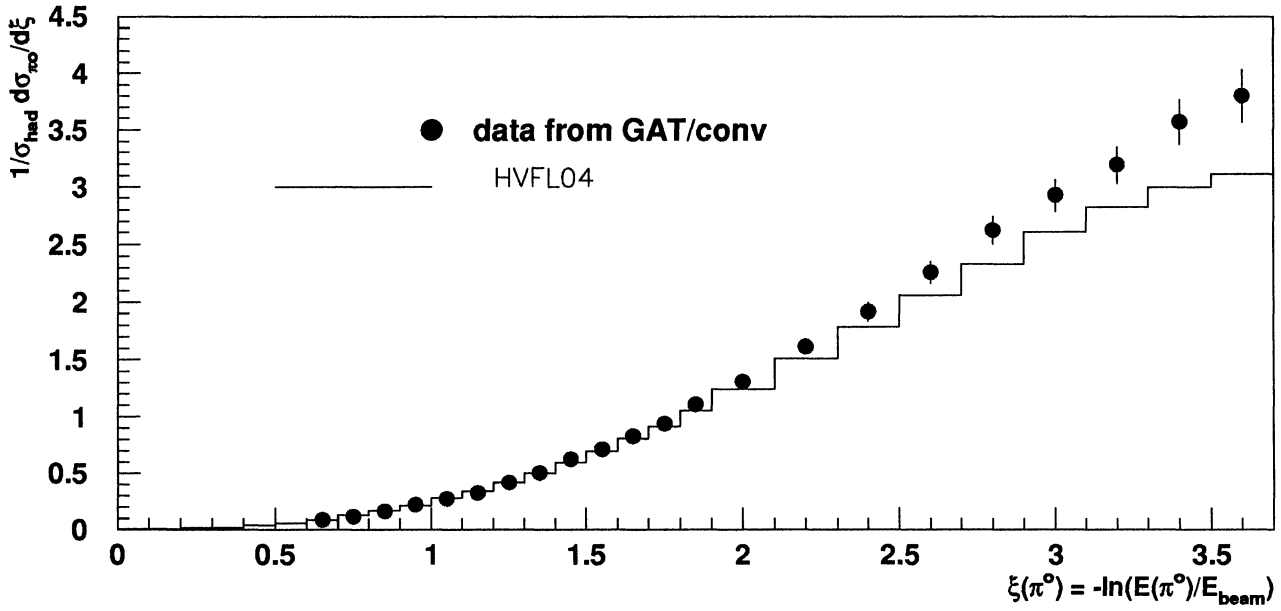


fig. 9.a

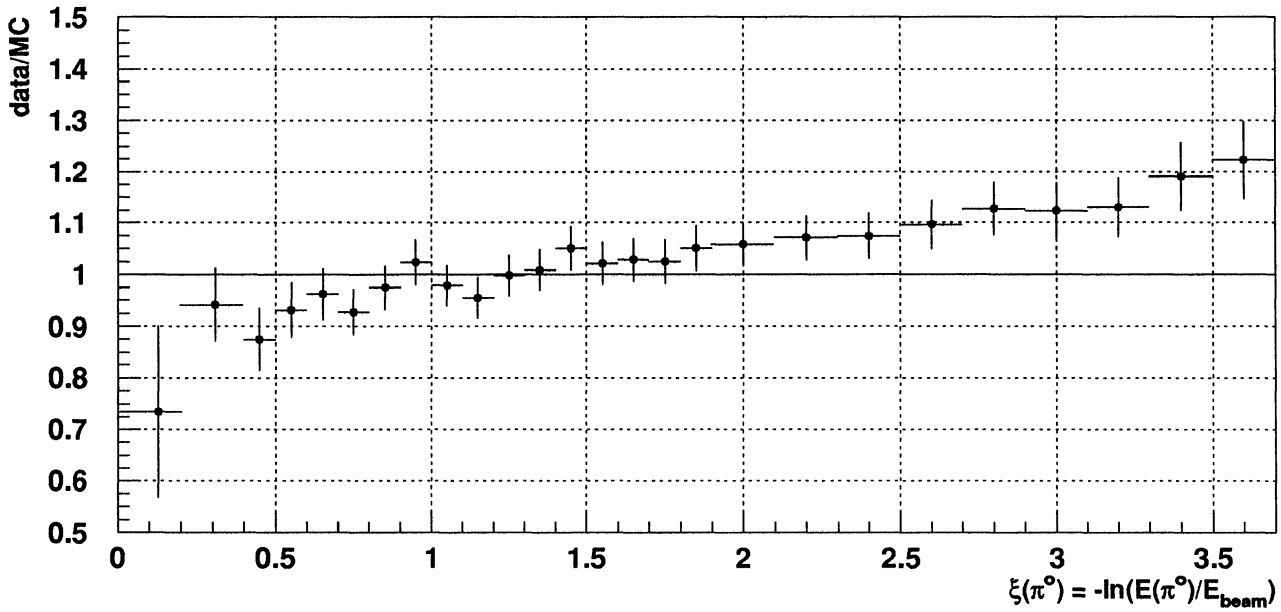


fig. 9.b: ratio data/generator HVFL04

# fig. 10: $\pi^o$ Pt spectrum (stat. err. only)

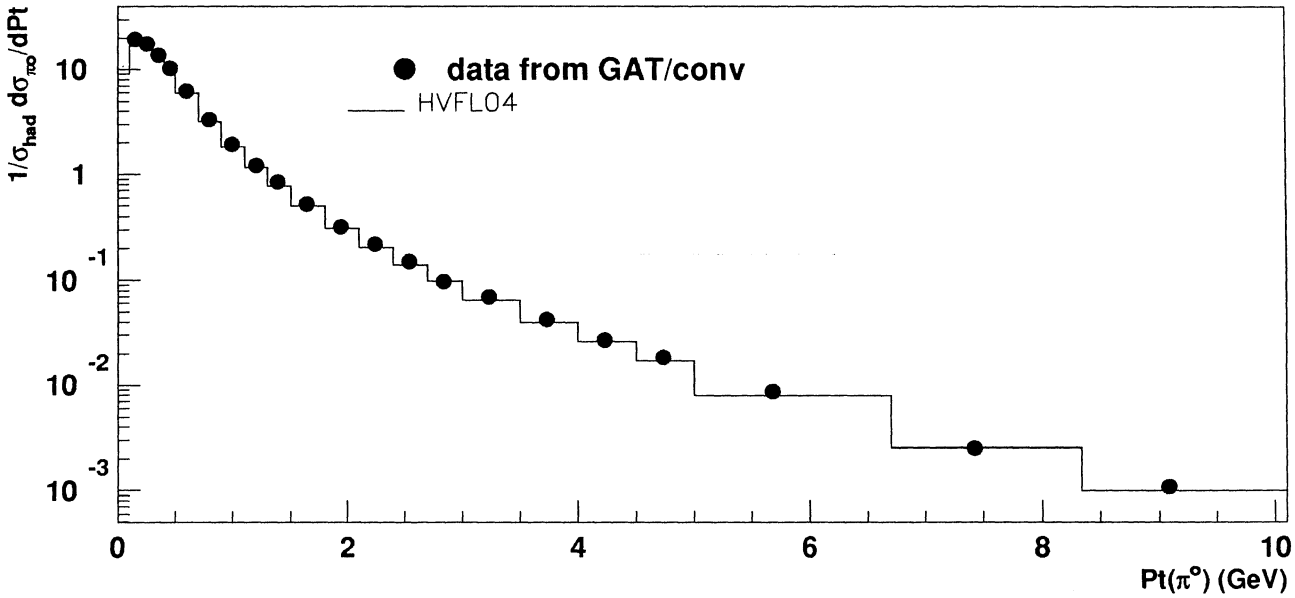


fig. 10.a

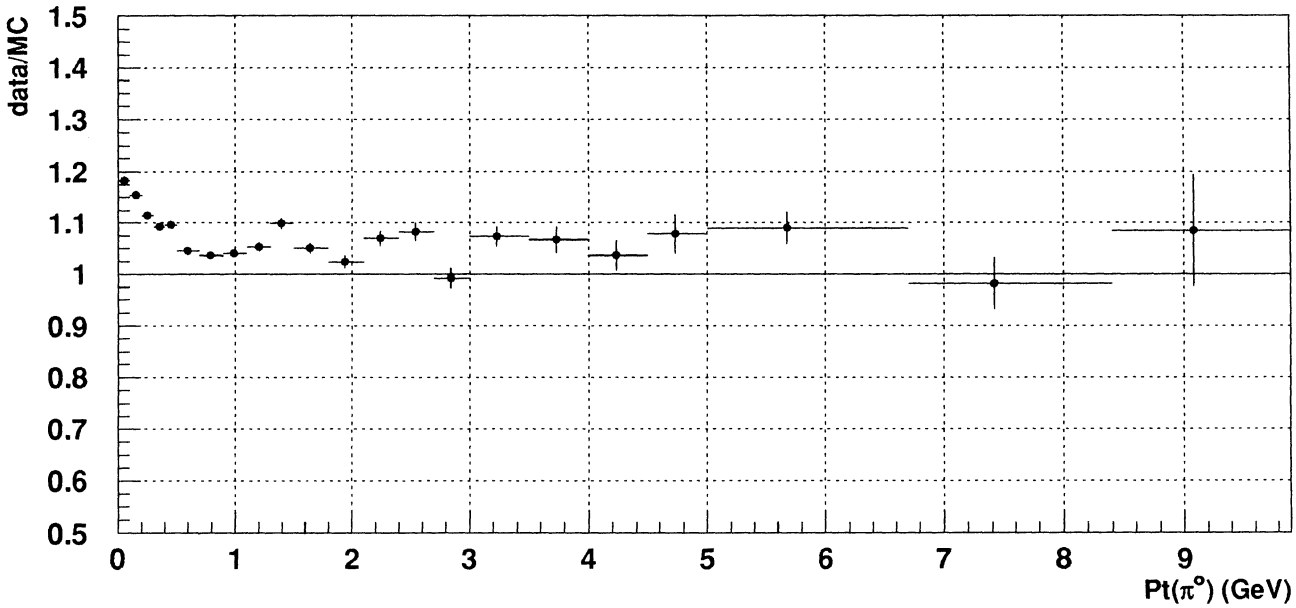


fig. 10.b: ratio data/generator HVFL04

# fig. 11: $\pi^o$ rapidity spectrum (stat. err. only)

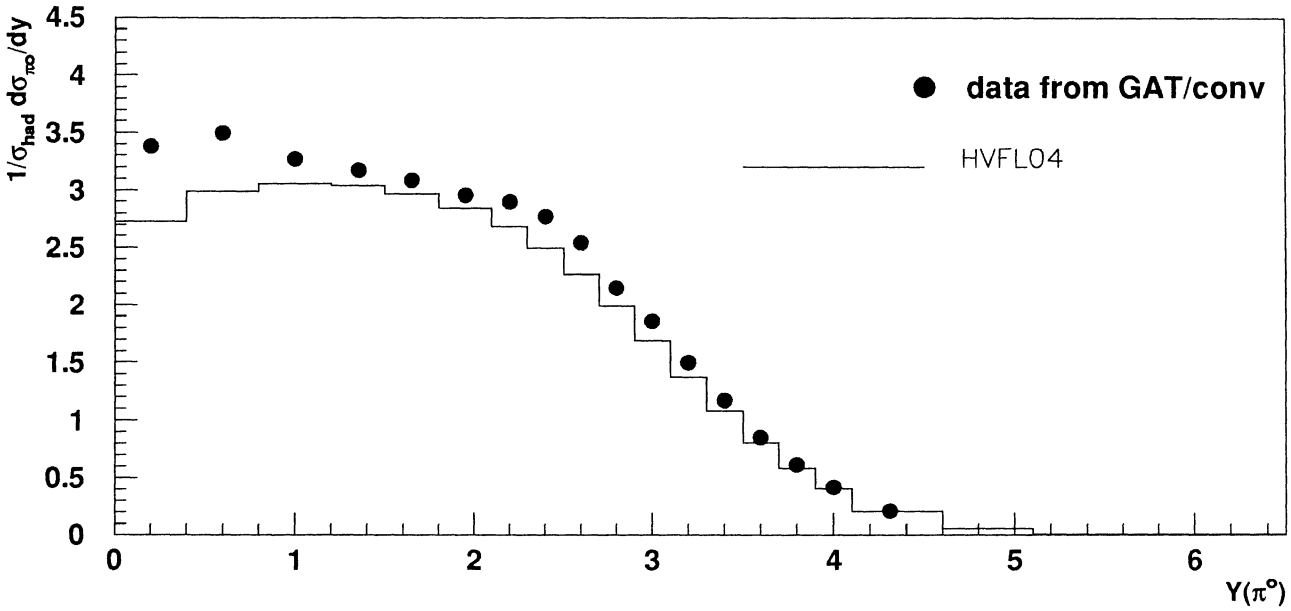


fig. 11.a

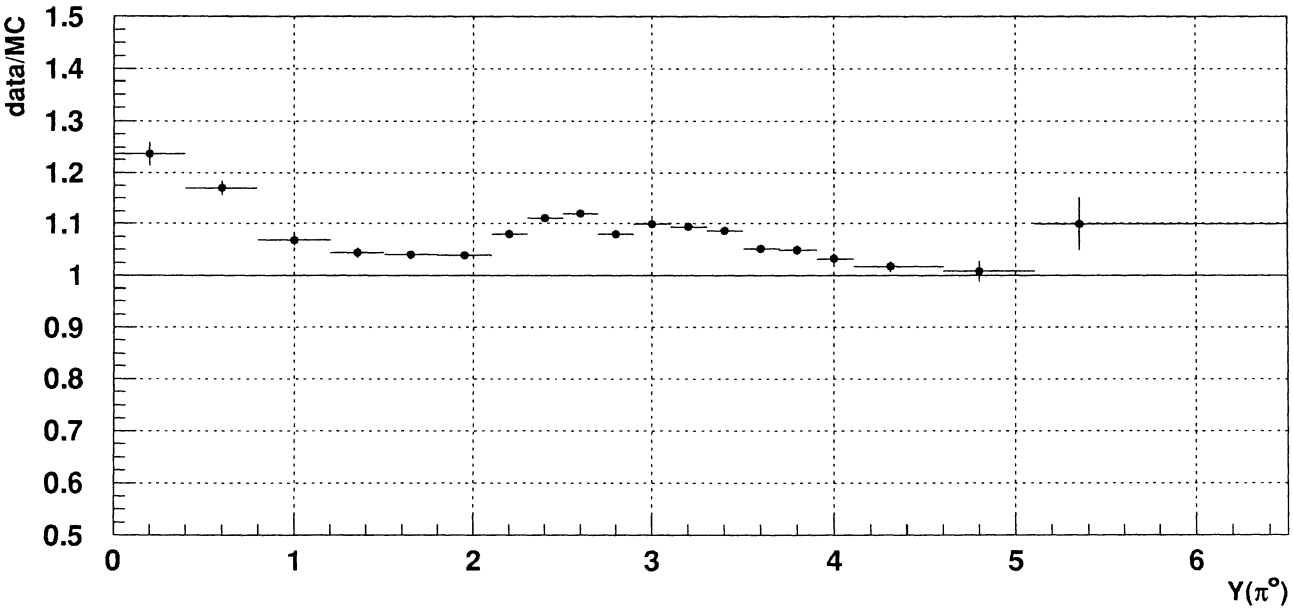


fig. 11.b: ratio data/generator HVFL04

# fig. 12: fit results (GAT/GAT analysis)

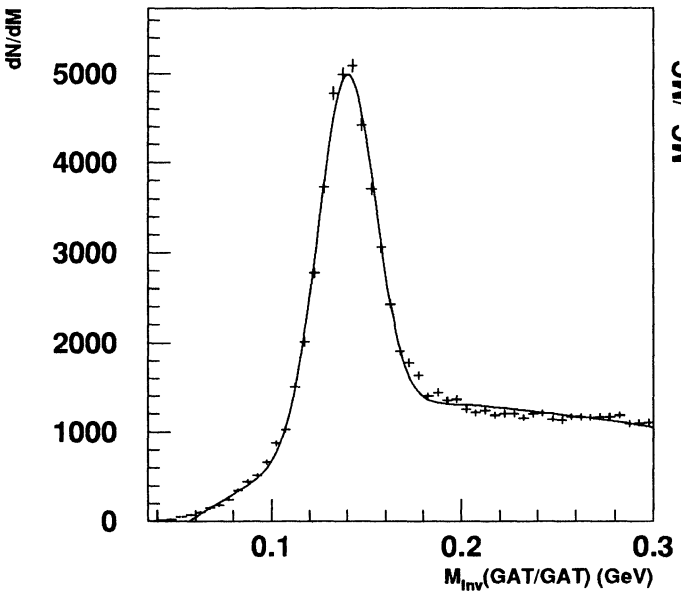


fig. 12.a: $0.2<x(\pi^0)<0.25$

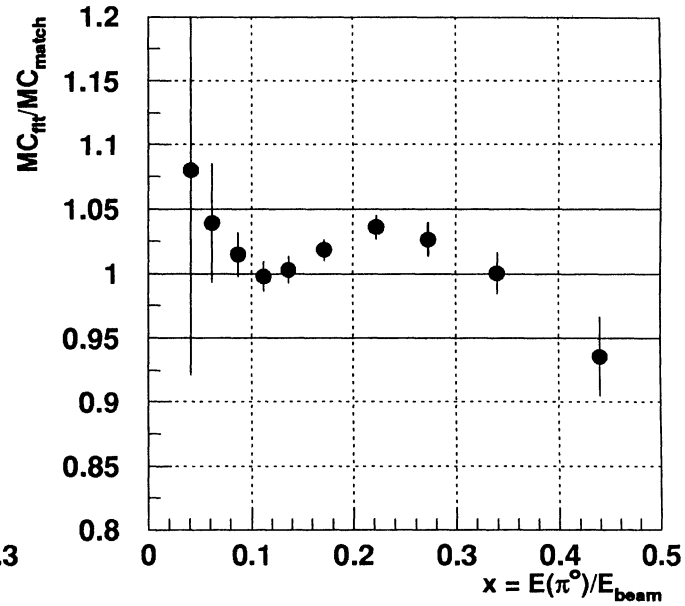


fig. 12.b: fitted/matched ratio

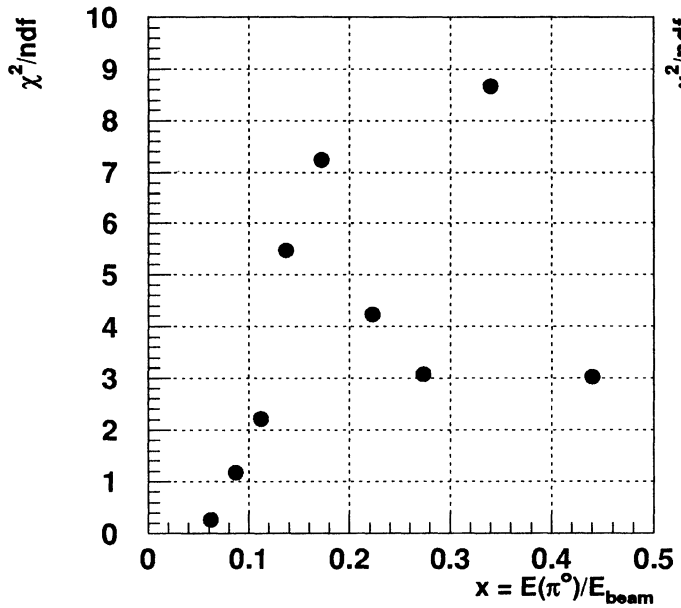


fig. 12.c: $\chi^2$/ndf data

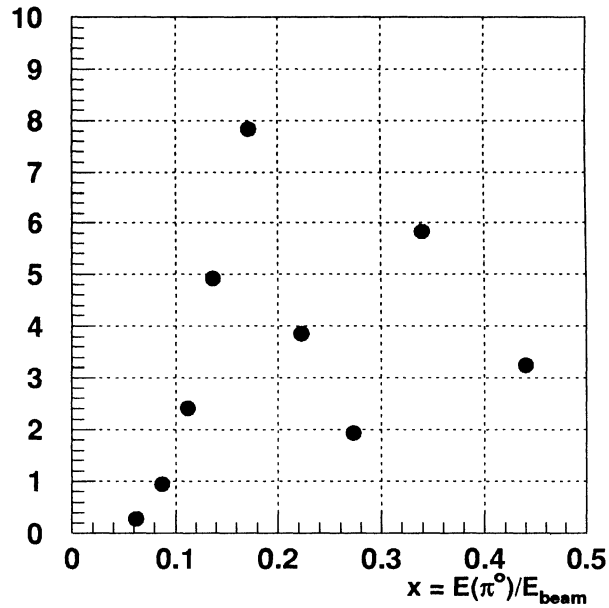


fig. 12.d: $\chi^2$/ndf MC

# fig. 13: $\pi^0$ fitted mass, width, S/(S+N) and global efficiency

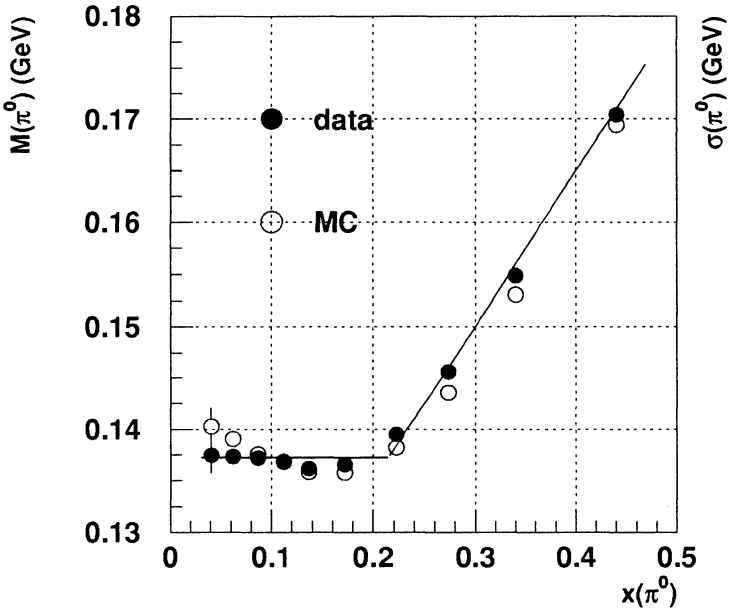


fig. 13.a: $\pi^\circ$ mass

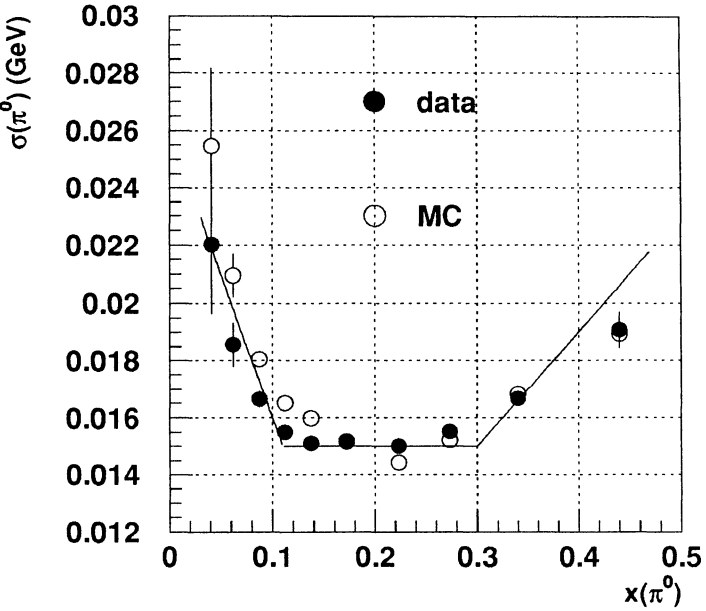


fig. 13.b: $\pi^\circ$ width

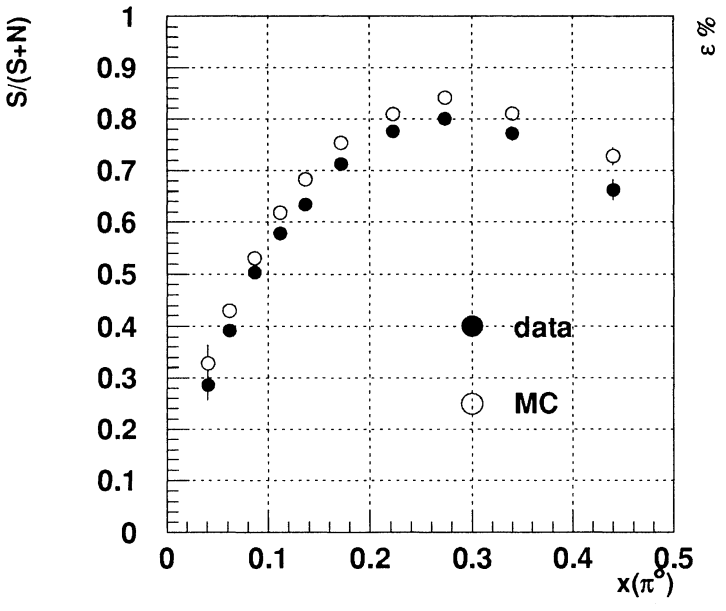


fig. 13.c: signal/(signal+noise)

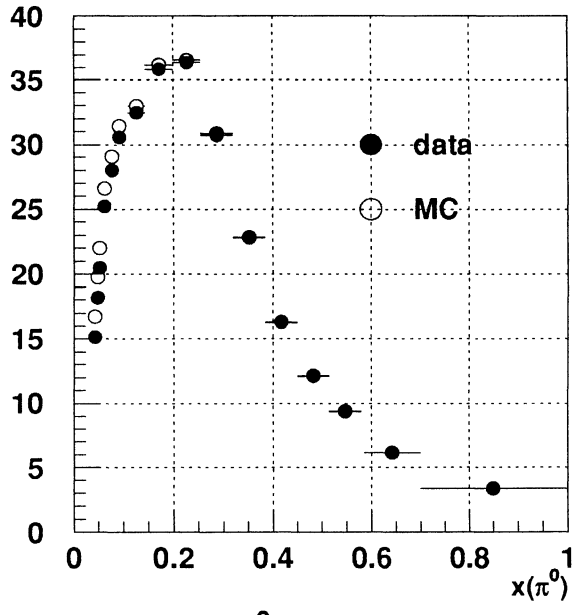


fig. 13.d: $\pi^0$ global efficiency

# fig. 14: $\pi^{o}\xi$ spectrum (stat. err. only)

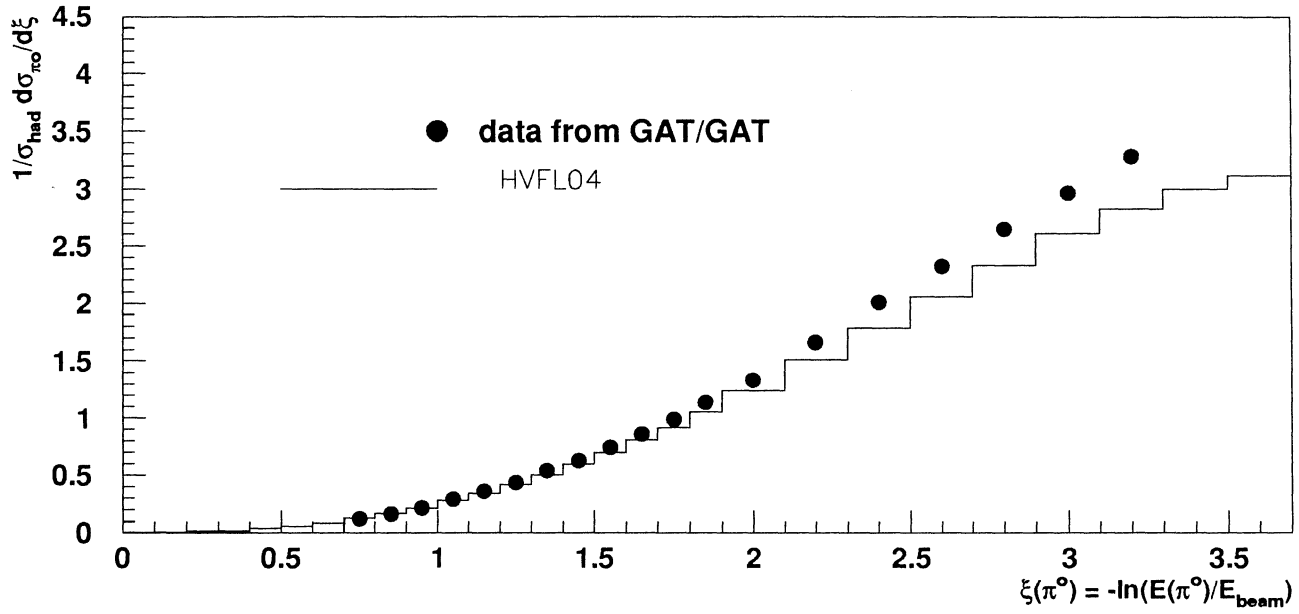


fig.14.a

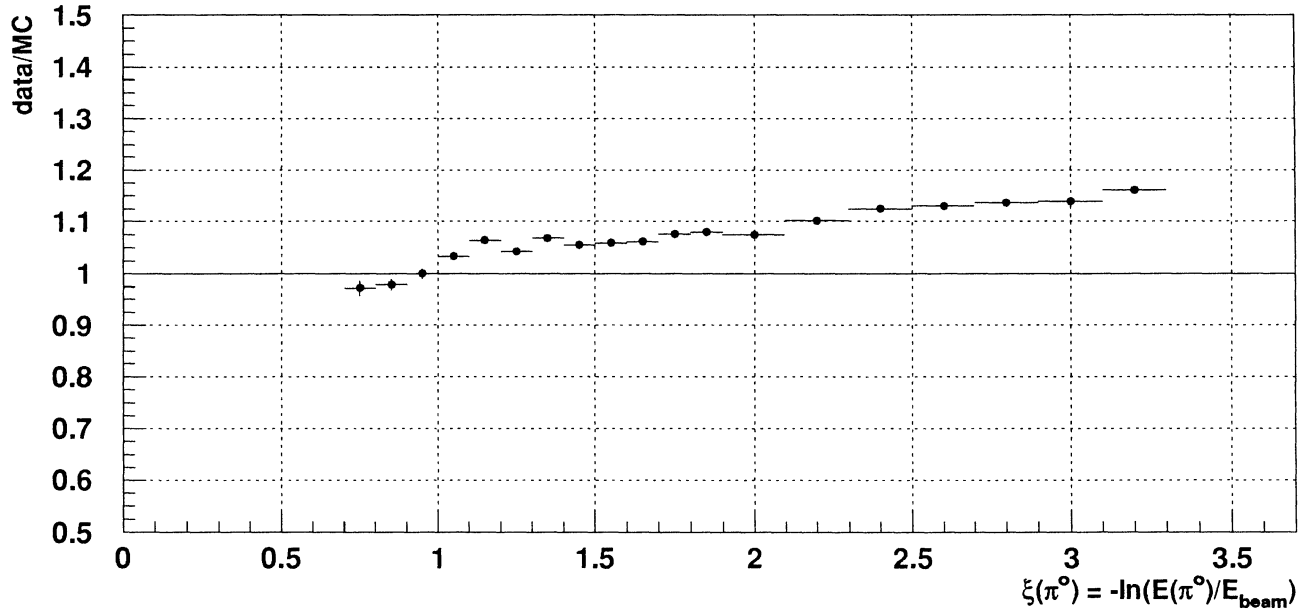


fig. 14.b: ratio data/generator HVFL04